RSC Advances

ROYAL SOCIETY OF CHEMISTRY

www.rsc.org/advances

Graphical Abstract (text)

Two series of bridged-phenoxido dinuclear Cu(II) complexes were synthesized, and structurally and magnetically characterized; doubly bridged $[Cu_2(\mu\text{-}L^{Cl}\text{-}O)(\mu\text{-}X)](ClO_4)_2$ (X = OH^-, $C_3H_3N_2^-$, $O_2P(OC_6H_5)_2^-$) and singly bridged $[Cu_2(\mu\text{-}L^{R}\text{-}O)(X)_2]PF_6 \cdot 2CH_3CN$ (R = Cl, CH_3 and X = dca) complexes.

Graphical Abstract (Pictogram)

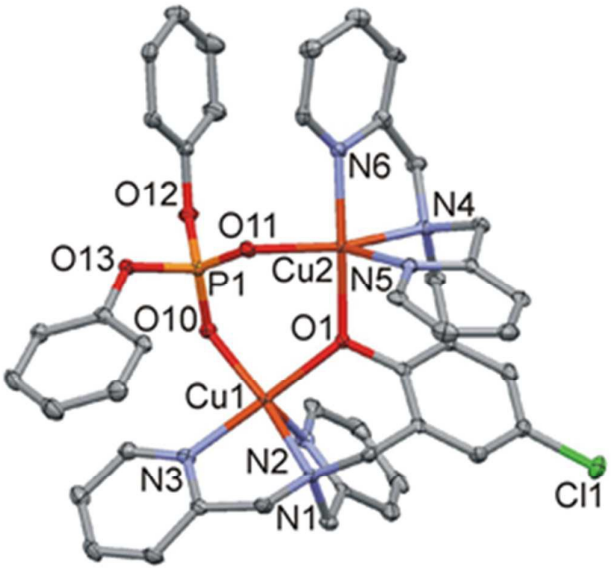

Synthesis, structure and magnetic characterization of dinuclear copper(II) complexes bridged by bicompartmental phenolate

Salah S. Massoud,[*a] Thomas Junk,[a] Febee R. Louka,[a] Radovan Herchel,[b] Zdeněk Trávníček,*[b] Roland C. Fischer,[c] Franz A. Mautner,*[d]

[a]*Department of Chemistry, University of Louisiana at Lafayette, Lafayette, LA 70504, U. S. A.*

[b]*Department of Inorganic Chemistry & Regional Centre of Advanced Technologies and Materials, Faculty of Science, Palacký University, 17. listopadu 12, CZ-77146 Olomouc, Czech Republic*

[c]*Institut für Anorganische Chemische, Technische Universität Graz, Stremayrgasse 9/V, A-8010 Graz, Austria*

[d]*Institut für Physikalische and Theoretische Chemie, Technische Universität Graz, Stremayrgasse 9/II, A-8010, Graz, Austria*

Received: **Accepted:**

Keywords: Copper / Dinuclear complexes / Bridged phenolate / Crystal structures / Magnetic properties/

* To whom correspondence should be addressed. E-mail: ssmassoud@louisiana.edu,Tel. +01 337-482-5672, Fax: +01 337-482-5676 (S. S. Massoud); E-mail: zdenek.travnicek@upol.cz, Tel. +420 585-634-352, Fax: +420 585-634-954 (Z. Trávníček); E-mail: mautner@tugraz.at, Tel. ++43 316-4873-8234, fax: ++43 316-4873-8225 (F.A. Mautner).

ABSTRACT:

The reaction of Cu(II) salts with the bicompartmental 2,6-bis[bis(2-pyridylmethyl)aminomethyl]-4-chlorophenol (L^{Cl}-OH) ligan afforded four new dinuclear bridged phenoxido Cu(II) complexes. Three doubly bridged complexes namely $[Cu_2(\mu\text{-}L^{Cl}\text{-}O)(\mu\text{-}X)](ClO_4)_2$ (**1**: X = OH^-, **3**: X = $O_2P(OC_6H_5)_2^-$) and **2**: $[Cu_2(\mu\text{-}L^{Cl}\text{-}O)(\mu\text{-}pz)(ClO_4)]ClO_4$ (**2**) where pz = pyrazolyl anion, and one singly bridged-phenoxido, $[Cu_2(\mu\text{-}L^{Cl}\text{-}O)(dca)_2]PF_6 \cdot 2CH_3CN$ (**4**$\cdot 2CH_3CN$) (dca = dicyanamide anion). A complex similar to **4** was also obtained with 2,6-bis[bis(2-pyridylmethyl)aminomethyl]-4-methylphenol (L^{Me}-OH), $[Cu_2(\mu\text{-}L^{Me}\text{-}O)(dca)_2]PF_6 \cdot 2CH_3CN$ (**5**$\cdot 2CH_3CN$) where in both cases dca are acting as terminal monodentate ligands. The complexes were structurally charaterized by various spectroscopic techniques (IR, UV-VIS and ESI-MS) and by single crystal crystallography. Magnetic susceptibilty measurements at variable temperature revelaed strong to very strong antiferromagentic coupling (AF) in the doubly bridged complexes **1-3** and very weak AF interaction in the dicyanamido compounds **4** and **5**. The DFT calculations for the coupling constants, *J* were in agreement with the experimentally observed behvior. The trend in magnetic properties was attributed to the strength of overlap between the orbitals ($d_{x2\text{-}y2}/d_{x2\text{-}y2}$ vs. $d_{z2}/d_{x2\text{-}y2}$ vs. d_{z2}/d_{z2}) resulting from trigonal bipyramidal (TBP) or square pyramidal (SP) geometries.

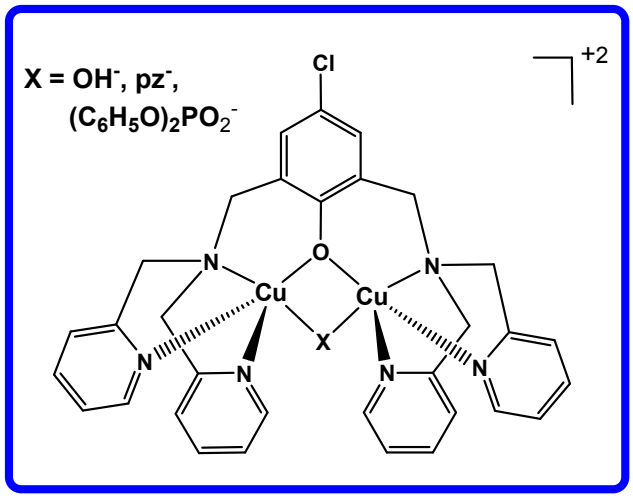

INTRODUCTION

A variety of compartmental ligands based on phenolic compounds which possess two symmetrical and asymmetrical pendant chelating arms attached to the 2- and 6-positions of the phenol ring have been synthesized.[1-11] These ligands are known to accommodate two homo- or hetero-metallic *3d* metal ions and hence producing dinuclear metal complexes bridged by the deprotonated phenolic group and in some cases by one or two other groups such as acetate, benzoate or hydroxide ions.[4-25] In many of these compounds, the coordination environment around the central metal ions is "*coordinatively unsaturated*" and/or the metal ion(s) is coordinated to "*weakly bound*" ligand(s).[1,2,4-6,10-13] This property made this class of compounds to serve as good candidates to mimic biological systems and as a consequence they have been extensively employed to elucidate the structural spectroscopic parameters and to mimic the mechanism of metalloenzymes in catecholase oxidases, Mn catalases, metallo-β-lactamases (MβL)[7,13,26-30] and particularly in the hydrolytic systems.[8,21,31,32] These includes phosphodiester bonds of biomolecules such as DNA, purple acid phosphatases and Zn phosphesterases.[8,21,31-33]

In addition to the advantages of the compartmental dinuclear metal(II) complexes which derived from phenolic compounds in enhancing our understanding for the role of metal ions in the active sides of metalloenzymes, the compounds could provide interesting magnetic properties as a result of the magnetic coupling between the two paramagnetic metal centers ($3d^{7-9}$) bridged *via* the phenoxido group. The close proximity between the bridged metal ions, which is generally within the range of 2.9-4.0 Å provide an excellent pathway for strong antiferromagnetic interaction between the two metallic centers.[1,2,4,28,30,34,35] Also, the magnetic coupling between the two metal ions could be enhanced by inserting another bridging ligand which can further propagate the magnetic coupling.[4,28,30,34,35]

Herein, we report a continuation of our previous studies on dinuclear metal(II) based phenolate ligands.[1,2] Our discussion will be limited on symmetrical tetra-methyl pyridyl compounds namely bis[bis(2-pyridylmethyl)aminomethyl]-4-chlorophenol (L^{Cl}-OH) and bis[bis(2-pyridylmethyl)aminomethyl]-4-methylphenol (L^{Me}-OH) which are illustrated in Chart 1. We report the synthesis, structure and magnetic characterization of three doubly bridged copper(II)-phenoxido complexes with OH^-, pyrazolyl anion (pz^-) and diphenylphosphate, as well as two singly bridged complexes with dicyanamide ion $N(CN)_2^-$ (dca).

Chart 1 Structural formula of *bis[bis(2-pyridylmethyl)aminomethyl]-4-substitutedphenol (L^R-OH)*

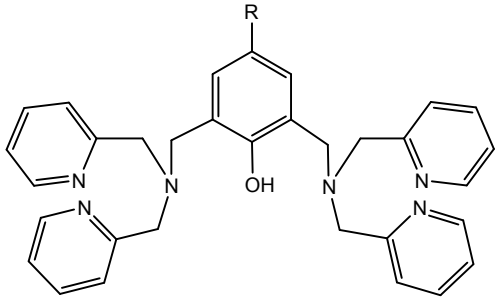

R = Cl (L^{Cl}-OH), Br (L^{Br}-OH),

CH_3 (L^{Me}-OH), $C(CH_3)_3$ ($L^{t\text{-}Bu}$-OH),

OMe (L^{OMe}-OH), F (L^{F}-OH)

Results and discussion

Synthesis of the complexes

The reaction of a methanolic solution of 2,6-bis[bis(2-pyridylmethyl)aminomethyl]-4-chlorophenol (L^{Cl}-OH) with two equivalents of $Cu(ClO_4)_2 \cdot 6H_2O$ in the presence Na_2CO_3, pyrazole (Hpz) and diphenyl phosphate afforded the dinuclear Cu(II) complexes $[Cu_2(\mu\text{-}L^{Cl}\text{-}O)(\mu_2\text{-}OH)](ClO_4)_2$ (**1**), $[Cu_2(\mu\text{-}L^{Cl}O)(\mu\text{-}pz)(ClO_4)]ClO_4$ (**2**) and $[Cu_2(\mu\text{-}L^{Cl}\text{-}O)(\mu\text{-}(O_2P(OC_6H_5)_2)](ClO_4)_2$ (**3**), respectively whereas the corresponding reactions of $Cu(NO_3)_2 \cdot 3H_2O$ and 2,6-bis[bis(2-pyridylmethyl)aminomethyl]-4-chlorophenol (L^{Cl}-OH) or 2,6-bis[bis(2-pyridylmethyl)aminomethyl]-4-methylphenol (L^{Me}-OH) with an aqueous solution of sodium dicyanamide (Nadca) resulted in the formation of $[Cu_2(\mu\text{-}L^{Cl}\text{-}O)(dca)_2]PF_6 \cdot 2CH_3CN$ **(4**$\cdot 2CH_3CN$**)** and $[Cu_2(\mu\text{-}L^{Me}\text{-}O)(dca)_2]PF_6 \cdot 2CH_3CN$ **(5**$\cdot 2CH_3CN$), respectively. The complexes were obtained in moderate to high yield (60–90%) in which the phenolic groups in all complexes and the pyrazine ligand in complex **2** were deprotonated. The isolated complexes were characterized by elemental microanalyses, molar conductivity, IR and UV-VIS spectroscopy, ESI-Ms spectrometry, and single crystal X-ray crystallography. The magnetic properties of the complexes were determined at variable temperature. The molar conductivities of the complexes **1-3** (Λ_M = 267-298 $\Omega^{-1}cm^2mol^{-1}$) as measured in CH_3CN were consistent with 1:2 electrolyte, whereas values of 161 and 179 $\Omega^{-1}cm^2mol^{-1}$ determined in complexes **4** and **5** are typical for 1:1 electrolytic behavior. The 1:2 electrolytic nature of complexes **1-3** is clearly obvious from their structural compositions which were also confirmed by the presence of extra bridges of mononegtative anions (OH^-, pz^- or $(C_6H_5O)_2PO_2^-$) in the bridged-phenoxido complexes $[Cu_2(\mu\text{-}L^{Cl}\text{-}O)(\mu\text{-}OH)](ClO_4)_2$

(**1**), $[Cu_2(\mu\text{-}L^{Cl}O)(\mu\text{-}pz)(ClO_4)]ClO_4$ (**2**) and $[Cu_2(\mu\text{-}L^{Cl}\text{-}O)(\mu\text{-}(O_2P(OC_6H_5)_2))](ClO_4)_2$ (**3**) (see X-ray section).

In the complexes **1**-**3**, the two Cu(II) ions are doubly bridged by the phenoxido group and a hydroxido group in **1**, pyrazolyl and diphenylphosphate anions in **2** and **3**, respectively. Bridged phenoxido complexes similar to **1** have been previously obtained in similar class of ligands.[5,28,36] Interestingly, although doubly-bridged mono(diphenylphosphato) complex **3** was isolated here, doubly-bridged bis(diphenylphosphato) complex was reported with Co(II), $[Co_2(\mu\text{-}L^{t\text{-}Bu}\text{-}O)(\mu\text{-}(O_2P(OC_6H_5)_2))](ClO_4)_2$.[37] Attempts made to synthesize the corresponding bis(4-nitrophenylphosphato) (BNP) of **3** were unsuccessful, most likely due to the rapid hydrolysis of BNP under the reaction conditions. Similarly attempts made to synthesize the bridged-azido or bridged-dicyanamido complexes were completely failed and instead, only the bridged-phenoxido complexes $[Cu_2(L^{Me}O)(N_3)_2]ClO_4$[2] and $[Cu_2(\mu\text{-}L^{R}\text{-}O)(dca)_2]PF_6\cdot 2CH_3CN$ (**4**, R = Cl; **5**, R = Me) were produced in which N_3^- and dca were acting as simple monodentate ligands.

IR spectra of the complexes

The IR spectra of the perchlorate complexes **1**-**3** displayed the ν(Cl-O) band as broad strong absorption around 1092 cm^{-1} as in complex **1** or split of the band into two or three bands over the range 1090-1120 cm^{-1} as observed in complexes **2** and **3**, respectively. The broadening or split of the ν(Cl-O) band is attributed to the reduction of the ClO_4^- ion symmetry from T_d to $C_{3\upsilon}$ or $C_{2\upsilon}$ symmetries as a result of the involvement of the counter ClO_4^- ion in H-bonding with the ligand or its presence in a distorted location. The dicyanamido hexafluorophoshate complexes **4** and **5** displayed strong absorption band around 840 cm^{-1}, due to ν(P-F). The latter two complexes showed two series of bands: a strong absorption in the 2160-2180 cm^{-1} region corresponding to $\nu_s(C\equiv N)$ and two weak to medium absorption bands in the 2220-2290 cm^{-1} region corresponding to $\nu_{as}(C\equiv N)$, and $\nu_s + \nu_{as}(C\equiv N)$[38] and these were in agreement with those observed in other monodentate dicyanamido complexes.[39] The frequencies of these peaks were shifted to higher values compared to the corresponding peaks observed in the free dca in its sodium salt (2129, 2232 and 2286 cm^{-1}) indicating its coordination. The bridged hydroxido complex **1**, revealed the stretching frequency ν(O-H) band at 3429 cm^{-1}. The complexes also displayed a series of weak to medium intensity bands over the 1610-1440 cm^{-1} region which are characteristic of the bis(pyridyl) moieties[40] and C=C of the phenolate group.

Electronic spectra of complexes

The acetonitrile spectra of copper complexes under investigation revealed the presence of two broad maxima over the wavelength regions 440-480 and 700-810 nm. The former band in the 440-480 nm region observed in complexes **2**-**4**, most likely corresponds to L→M CT transition between the bridged phenoxido and copper ions. The second observed broad band (710-810 nm region, ε = 140-200 $M^{-1}cm^{-1}$) is characteristic for Cu(II) *d-d* transition in *five-coordinate* complexes. The long wavelength position of this band suggests a distorted square pyramidal (SP) stereochemistry around the central Cu(II) ions. It is well established that *five-coordinate* SP Cu(II) complexes are most likely producing a broad band in the visible region which occasionally may or may not be associated with a low-energy shoulder at λ > 800 nm. This band results from *dxz, dyz* → dx^2-y^2 transition.[41,42] Similar UV-Vis spectral features have been previously reported in related μ-phenoxido dicopper(II) complexes.[1,2,28,43] Thus, based on the above criterion in CH_3CN solution, the complexes under investigation adopt distorted SP geometry around the central Cu(II) atoms This assignment in solution was in agreement with those obtained by single crystal X-ray crystallography.

Mass spectra of complexes

ESI-MS spectra of the chlorophenolate complexes **1**-**4** and the methylphenolate complex **5**, recorded in acetonitrile and all are shown in Figs S1†-S5† (ESI†), displayed some general characteristic features which provide qualitative information about their compositions. The mass spectra of the complexes **1**, **3** and **4** showed two major peaks at *m/z* = 835.059±0.001 (this was observed at *m/z* = 821.020 for complex **2**) and 767.071±0.002. The former peak may result from the formation of a species with additional coordination of OH^-/H_2O/MeCN to the Cu(II) centers such as $[Cu_2(L^{Cl}O)(OH)(H_2O)(MeCN)_3]^{2+}$ (calcd *m/z* = 835.158) in complexes **1**, **3** and **4**, whereas the corresponding peak observed in complex **2** (*m/z* = 821.020) could be assigned to $[Cu_2(L^{Cl}O)(pz)(H_2O)(MeCN)]^{2+}$ (calcd *m/z* = 821.317). The second major peak which was detected in complexes **1**-**4** at 767.071±0.002 could be attributed to the fragments $\{[Cu_2(L^{Cl}O)(H_2O)]^{3+}+2Cl^-+H^+\}^{2+}$ (calcd *m/z* = 767.094) in complexes **1**-**3** and $\{[Cu_2(L^{Cl}O)(OH)(H_2O)_3]^{2+}+F^-+H^+\}^{2+}$ (calcd *m/z* = 767.031) in complex **4**. Similar peaks were observed in complex **5** at *m/z* = 813.113 and 747.125 corresponding to the species $[Cu_2(L^{Me}O)(OH)_2(MeCN)_3]^+$ (calcd *m/z* = 813.917) and $\{[Cu_2(L^{Me}O)(OH)(H_2O)_3]^{2+}+F^-\}^+$ (calcd *m/z* = 746.798), respectively. The spectra revealed a distinct

peak at *m/z* = 361.035±0.001 for complexes **1-4** and at 351.063 for complex **5** due to doubly charged ions. These were assigned to the fragment $[Cu_2(L^RO)(H_2O)(HCN)]^{3+}$ (calcd *m/z* = 361.103 for R = Cl in complexes **1-4** and *m/z* = 350.894 for R = Me in complex **5**). In addition to these peaks, the perchlorate complexes **1-3**, and the hexafluorophosphate complexes **4** and **5** displayed an *m/z* peak at 98.949 (100%) and 144.949 (100%) attributable to the ClO_4^- (calcd *m/z* 99.451) and PF_6^- (calcd *m/z* 144.642) ions, respectively.

Species with additional coordination such as those observed in the above complexes when MeCN was used as a solvent in measuring the mass spectra, have been recently reported in some dinuclear metal(II) complexes based phenolate.[2, 44]

Crystal structures of the complexes

$[Cu_2(\mu\text{-}L^{Cl}O)(\mu\text{-}OH)](ClO_4)_2$ (1). The molecular structure of **1** consists of dinuclear $[Cu_2(L^{Cl}O)(OH)]^{2+}$ complex cations and ClO_4^- counter ions. A Perspective view of the complex cation together with partial atom numbering schemes is given in Fig. 1, and selected bond parameters are summarized in Table S1† (ESI†). Each Cu(II) center within the dinuclear complex cation is penta-coordinated by three *N*-donor atoms of one bis-pyridylamino group, the bridging O(1) atom of central 4-chlorophenolate moiety and O(10) oxygen atom of bridging hydroxy group. Both CuN_3O_2 chromophores adopt distorted SP geometry [τ-values: 0.15 and 0.14, for Cu(1) and Cu(2), respectively][45] with N(3) and O(1) atoms in apical sites [Cu(1)-N(3) = 2.205(5), Cu(2)-O(1) = 2.200(4) Å]. The basal Cu-N/O bond distances are in the range from 1.932(3) to 2.044(5) Å. The Cu(1)···Cu(2) intra-dimeric distance is 3.0297(13) Å, and the shortest inter-dimer metal-metal separation is 7.166(2) Å. The Cu(1)-O(1)-Cu(2), Cu(1)-O(10)-Cu(2), O(1)-Cu(1)-O(10) and O(1)-Cu(2)-O(10) bond angles are 93.36(15), 103.29(18), 84.49(15) and 78.27(14)°, respectively. Cu(2) forms an additional semi-coordinative bond to O(6A) atom of partially disordered perchlorato anion [Cu(2)-O(6A) (x,1/2-y,1/2+z) = 2.719(8) Å] (Fig. S6†).

Please insert Figure 1 close to here

$[Cu_2(\mu\text{-}L^{Cl}O)(\mu\text{-}pz)(ClO_4)]ClO_4$ (2). The molecular structure of **2** consists of dinuclear $[Cu_2(L^{Cl}O)(C_3H_3N_2)(ClO_4)]^+$ complex cations and ClO_4^- counter ions. A perspective view of the complex cations together with partial atom numbering scheme is given in Fig. 2, and selected bond

parameters are summarized in Table S2†. Cu(1) has a 4+1+1 geometry formed by three N donor atoms of one bis-pyridylamino group, N(7) of a bridging single deprotonated pyrazole, the bridging O(1) atom of central 4-chlorophenolate moiety and O(2) oxygen atom of a terminal perchlorate group. The four short Cu(1)-N bond lengths are in the range from 1.957(5) to 2.020(6) Å. The axial Cu(1)-O(1), Cu(1)-O(2) and O(1)-Cu(1)-O(2) bond parameters are 2.227(4) Å, 2.769(7) Å and 157.87(17)°, respectively. Cu(2) is penta-coordinated by three N donor atoms of second disordered bis-pyridylamino group, N(8) of a bridging single pyrazolyl anion, and the bridging O(1) atom of central 4-chloro-phenolate moiety. The CuN_3O_2 chromophore adopts a distorted TBP geometry [τ-value: 0.73 (for N5A) or 0.78 (for N5B)].[45] The axial sites are occupied by N(4) and N(8) atoms [Cu(2)-N(4) = 2.020(6) Å, Cu(2)-N(8) = 1.994(7) Å, N(4)-Cu(2)-N(8) = 174.1(2)°]. The equatorial Cu(2)-N/O bond distances are in the range from 1.997(10) to 2.186(11) Å. The Cu(1)···Cu(2) intra-dimeric distance is 3.4635(10) Å, and the shortest inter-dimer metal-metal separation is 8.0887(11) Å. The Cu(1)-O(1)-Cu(2) bond angles is 108.85(18)°. Packing plot of the compound is shown in Fig. S7†.

Please insert Figure 2 close to here

$[Cu_2(\mu\text{-}L^{Cl}O)(\mu\text{-}O_2P(OC_6H_5)_2)](ClO_4)_2$ (3). The molecular structure of **3** consists of dinuclear $[Cu_2(L^{Cl}O)(O_2P(OC_6H_5)_2)]^{2+}$ complex cations and ClO_4^- counter ions. A perspective view of the complex cation together with partial atom numbering scheme is given in Fig. 3 and selected bond parameters are summarized in Table S3†. Each Cu(II) center within the dinuclear complex cation is penta-coordinated by three *N*-donor atoms of one bis-pyridylamino group, the bridging O(1) atom of central 4-chlorophenolate moiety and an oxygen atom of bridging $(PO_2)(OC_6H_5)_2$ group. Both CuN_3O_2 chromophores adopt distorted SP geometry [τ-values: 0.09 and 0.16, for Cu(1) and Cu(2), respectively][45] with N(2) and N(5) atoms in apical sites [Cu(1)-N(2) = 2.140(4), Cu(2)-N(5) = 2.173(4) Å]. The basal Cu-N/O bond distances are in the range from 1.959(3) to 2.054(4) Å. The Cu(1)···Cu(2) intra-dimeric distance is 3.5884(10) Å, and the shortest inter-dimer metal-metal separation is 6.7623(12) Å. The Cu(1)-O(1)-Cu(2), Cu(1)-O(10)-P(1), and Cu(2)-O(11)-P(1) bond angles are 126.90(17), 124.1(2) and 120.1(2)°, respectively. Packing plot of compound **3** is shown in Fig. S8†.

Please insert Figure 3 close to here

$[Cu_2(\mu\text{-}L^{Cl}O)(dca)_2]PF_6\cdot 2MeCN$ (4·2MeCN**)** and **$[Cu_2(\mu\text{-}L^{Me}O)(dca)_2]PF_6\cdot 2MeCN$ (5**·2MeCN**)**. The molecular structures of these molecules consist of dinuclear complex cations $[Cu_2(L^{Cl}O)(dca)_2]^+$ or $[Cu_2(L^{Me}O)(dca)_2]^+$, PF_6^- counter ions and MeCN lattice solvent molecules. Perspective views of the crystal structures together with partial atom numbering schemes are depicted in Fig 4, and selected bond parameters are presented in Tables S4† and S5†, respectively. Each Cu(II) center within a dinuclear complex cation is penta-coordinated by three N donor atoms of one bis-pyridylamino group, a terminal dicyanamide anion in basal sites, and the bridging O(1) atom of central 4-substituted-phenolate moiety, which occupies the axial position of the distorted square pyramids [τ-values: 0.05 and 0.07 for **4** and 0.05 and 0.04 for **5**].[45] The corresponding axial Cu-O(1) bond distances are 2.190(5), 2.190(5), 2.170(2) and 2.172(2) Å, respectively. The basal Cu-N bond distances are in the range from 1.961(5) to 2.058(6) Å. The Cu(1)-O(1)-Cu(2) bridging bond angles are 136.82(17) and 137.65(8)°, respectively. The intra-dimeric metal···metal distances are 4.0727(12) and 4.0492(5) Å, and the shortest inter-dimer metal-metal separations are 8.3646(12) and 8.3684(6) Å, for **4** and **5**, respectively (Figs S9† and S10†). The terminal dicyanamido ligands have the following bond parameters: C-N(nitril): 1.142(4) – 1.174(8) Å, C-N(amide): 1.288(9) – 1.342(11) Å, N-C-N: 173.5(3) – 175.0(9)°, C-N-C: 117.8(7) – 119.9(3)°, Cu-N-C: 160.8(3) – 164.7(3)°.

Please insert Figure 4 close to here

Magnetic properties of complexes

The analysis of the magnetic data was based on the spin Hamiltonian for dinuclear system of the form

$$\hat{H} = -J\left(\vec{S}_1 \cdot \vec{S}_2\right) + \sum_{i=1}^{2} \mu_B B g_i \hat{S}_{i,z} \qquad (1)$$

where the isotropic exchange (J) and Zeeman term (g) are included. Then, the molar magnetization can be easily calculated using the following analytical formula[46]

$$M_{mol} = \mu_B g N_A \frac{e^{(J+x)/kT} - e^{(J-x)/kT}}{1 + e^{(J+x)/kT} + e^{J/kT} + e^{(J-x)/kT}} \qquad (2)$$

where $x = \mu_B g B$.

Moreover, the small amount of monomeric paramagnetic impurity (PI) which accounts for increase of molar magnetization (mean susceptibility) at low temperatures was taken into consideration by Eq. 3

$$M_{sample} = (1 - x_{PI}) M_{mol} + 2 \cdot x_{PI} M_{PI} \qquad (3)$$

where M_{PI} was calculated using the Brillouin function. Both temperature and field dependent magnetic data of the studied compounds were included into fitting procedures.

The experimental magnetic data of **1** are depicted in Fig. 5. The theoretical effective magnetic moment μ_{eff} for two uncoupled $S_1 = S_2 = ½$ and $g = 2.0$ is 2.45 μ_B or for more typical value of g-factor for copper(II) compounds equaled to 2.2 is $\mu_{eff}/\mu_B = 2.69$. The room temperature value of μ_{eff} is 2.06 μ_B and is decreasing on lowering the temperature. The presence of two maxima of M_{mol} vs. T curve located at $T_{max,1} = 52.3$ K and $T_{max,1} = 213.3$ K suggests that most likely the sample was contaminated by unidentified impurity, which was not detected by standard physico-chemical methods Probably, it should be mentioned that several independently prepared batches of the complex were tested and same result was obtained. However, there is a simple formula derived for dinuclear species which can be used to estimate J-value as [46]

$$|J| / kT_{max} = 1.599 \quad (4)$$

Then, the first maximum corresponds to $J_1 = -58.2$ cm^{-1}, while the second one to $J_2 = -237$ cm^{-1}. The J_1 spans the interval between DFT calculated values (see next section) $J^{Ruiz} = -43.1$ cm^{-1} and $J^{Yam} = -85.5$ cm^{-1}, so it can be suggested that J_1 matches the predicted magnetism of compound **1**, while the J_2 may be assigned to the unknown impurity.

Please insert Figure 5 close to here

Contrary to the case described above, the experimental magnetic data for **2** (Fig. 6) matches well with the expectations where the effective magnetic moment is close to 2.7 μ_B at 300 K and continuously decreases to 0.24 μ_B at 1.9 K. The maximum of M_{mol} vs. T curve is located at $T_{max} = 55.1$ K, which corresponds to $J = -61.2$ cm^{-1}. Fitting procedure, which was done according to eqs. 1-3, resulted in $J = -61.5$ cm^{-1}, $g = 2.14$, $\chi_{TIP} = 3.9 \cdot 10^{-9}$ m^{3}mol^{-1}, $\chi_{PI} = 0.85\%$, where χ_{TIP} represents the correction to the temperature-independent magnetism (TIP). The strong antiferromagnetic exchange in **3**, as compared to **2**, is simply evident by its experimental magnetic data (Fig. 7), where T_{max} located at 243 K was served as an estimate for $J = -270$ cm^{-1}. This value is close to that found by the fitting procedure: $J = -279$ cm^{-1}, $g = 2.17$, $\chi_{TIP} = 0.0 \cdot 10^{-9}$ m^{3}mol^{-1}, $x_{PI} = 2.60\%$.

Please insert Figures 6 and 7 close to here

For the remaining two dicyanamido compounds, $[Cu_2(\mu\text{-}L^R\text{-}O)(dca)_2]PF_6 \cdot 2CH_3CN$ (**4**: R = Cl; **5**: R = CH_3), DFT calculations predicted almost negligible antiferromagnetic exchange (see next section). Indeed, the effective magnetic moment is almost constant over the whole temperature range (the gradual increase of μ_{eff}/μ_B on heating in the case of **5** can be attributed to small amount of para/ferromagnetic impurity and due to temperature-independent magnetism). There is no maximum of M_{mol} vs. T curve, which suggests that the value of $|J|$ should be less than 2 cm^{-1}. This agrees well with the fitted values: J = -0.26 cm^{-1}, g = 2.15, χ_{TIP} = $1.0 \cdot 10^{-9}$ m^3mol^{-1} for **4** and J = -0.11 cm^{-1}, g = 2.08, χ_{TIP} = $1.9 \cdot 10^{-9}$ m^3mol^{-1} for **5**.

Please insert Figures 8 and 9 close to here

DFT calculations

Our previous study on dinuclear singly bridged-phenoxido metal(II) complexes showed that in the case of copper(II) complex of the type $[Cu_2(\mu\text{-}L^{Cl}\text{-}O)Cl_2]PF_6 \cdot 1/2MeOH$, there is a very weak antiferromagnetic exchange due to ineffective overlap of non-orthogonal magnetic orbitals.[1] In the present study there are additional bridging ligands in compounds **1-3**, therefore the DFT calculations were performed to reveal the effect of these extra bridging on the magnetic properties. Thus, we calculated the isotropic exchange parameters J using the ORCA 3.0 software for compounds **1-3** and extended the calculations also for compounds **4** and **5** for comparison purposes. Following our previous study[1] we used the B3LYP functional and def2-TZVP(-f) basis set to calculate the energy difference Δ, between high spin (HS) and broken-symmetry (BS) spin states:

$$\Delta = E_{BS} - E_{HS} \quad (5)$$

This energy difference is then used to calculate J-value for the dinuclear spin Hamiltonian defined as

$$\hat{H} = -J\left(\vec{S}_1 \cdot \vec{S}_2\right) \quad (6)$$

by both Ruiz's approach

$$J^{\text{Ruiz}} = 2\Delta / \left[(S_1 + S_2)(S_1 + S_2 + 1)\right] \quad (7)$$

and by Yamaguchi's approach

$$J^{\text{Yam}} = 2\Delta / \left[\left\langle S^2 \right\rangle_{\text{HS}} - \left\langle S^2 \right\rangle_{\text{BS}}\right] \quad (8)$$

The results of DFT calculations are summarized in Table 1 and illustrated in Fig 10. All the J-values were found negative and suggesting the presence of antiferromagnetic coupling ranging from

very weak (**5**) to very strong (**3**). In case of square-pyramidal geometry (SP) the unpaired electron resides in d_{x2-y2} orbitals, while the corresponding trigonal-bipyramid (TBP) geometry resulted in magnetic orbital based on d_z^2 (Cu2 in compound **2**). The smallest overlap $S_{\alpha\beta}$ between the non-orthogonal orbitals was found for **5** and the largest for **3**, which is in agreement with strength of antiferromagnetic exchange.

Please insert Table 1 and Figures 10-11 close to here

Careful inspection of literature showed that there are only four other examples similar to ours where the magnetic properties were studied for copper(II) dimers containing both L^R-OH and X ligands (Chart 1), namely $[Cu_2(\mu\text{-}L^{Me}O)(\mu\text{-}OH)](ClO_4)_2\cdot THF$ (**6**),[28] $[Cu_2(\mu\text{-}L^{tBu}O)(\mu\text{-}OCH_3)](ClO_4)_2\cdot H_2O$ (**7**),[34] $[Cu_2(\mu\text{-}L^{Me}O)(\mu\text{-}CH_3COO)](PF_6)_2$ (**8**),[4] and $[Cu_2(\mu\text{-}L^{tBu}O)(\mu\text{-}CH_3COO)](PF_6)_2$ (**9**)[47] with J^{mag} = -224, -312, -80, +30.8 cm^{-1}, respectively. The reported J^{mag} values were scaled according to the spin Hamiltonian definition in eq. 1. Interestingly, compounds **1, 6** and **7** have the same hydroxo/alkoxo-bridging groups (X = OH^-/CH_3O^-) and despite the fact that structural parameters defining the bridges, like Cu–O_{Ph}–Cu (93.45-95.66 °) and Cu–O_X–Cu (102.1-103.29 °) angles or Cu···Cu distances (2.966-3.030 Å) are almost the same (Table 1), the J^{mag} values vary significantly. More interesting is also the comparison of the J^{mag} values for acetato-bridged complexes **8** and **9**, which are structurally almost identical (Table 1), their reported magnetic exchanges are either antiferromagnetic or ferromagnetic. Therefore, we utilized the above described DFT procedure to calculate the magnetic exchange parameters also for compounds **6-9** in order to elucidate the observed large variations of the isotropic exchange parameters within this family of coordination compounds. The main results are listed in Table 1 and illustrated in Figs. 10 and 11. Within the structurally similar first group of compounds **1, 6** and **7**, it is obvious that the calculated strength of the antiferromagnetic exchange (J^{Ruiz}/J^{Yam}) increases with increasing the overlap of magnetic orbitals ($S_{\alpha\beta}$): $d_{x2-y2}/d_{x2-y2} < d_{z2}/d_{x2-y2} < d_{z2}/d_{z2}$. Thus, we may conclude that the main source of variation of magnetic properties in **1, 6** and **7** is due to the different geometry around the central copper ions (SP vs. TB). The large difference in J^{mag} for compounds **2** (J^{mag} = -61.5 cm^{-1}) and **3** (J^{mag} = -279 cm^{-1}) with the bridging ligands X (X = the pyrazolyl anion for **2** and diphenylphosphate anion for **3**) can be explained by the fact that in the case of the diphenylphosphato ligand, there is efficient overlap of orbitals (d_{x2-y2}/d_{x2-y2}) through both bridging ligands, whereas in compound **3**, the μ-

phenoxido ligand is ineffective for overlap of the d_{z2}/d_{x2-y2} orbitals and thus only the μ-pyrazolato ligand is the one that mediates magnetic exchange (Fig. 10). Next, in singly bridged-phenoxido compounds **4** and **5**, the d_{x2-y2}/d_{x2-y2} orbitals are lying in CuN_4 planes perpendicular to the Cu-O_{Ph} bond, which leads to their negligible overlap, and hence to a very weak antiferromagnetic exchange similar to the previously observed in $[Cu_2(\mu\text{-}L^{Cl}O)Cl_2]PF_6 \cdot ½MeOH$.[1] Finally, we would like to comment on the results of compounds **8** and **9**. In these compounds **8**, the magnetic orbitals have d_{x2-y2}/d_{x2-y2} character and their mutual orientation exclude their efficient overlap through the μ-phenoxido ligand and also through acetato ligand (Fig. 11), which results in calculated ferromagnetic exchange, J^{Ruiz}/J^{Yam} = 15.8/31.5 cm^{-1} for **8** and J^{Ruiz}/J^{Yam} = 26.9/53.8 cm^{-1} for **9** (Table 1). The variation in the calculated *J*-values in **8** and **9** can be most probably attributed to the small differences in orientation of acetato-ligand with respect to both CuN_2O_2 planes containing magnetic orbitals with d_{x2-y2}/d_{x2-y2} character.[48] This can be demonstrated by evaluating the angle between plane of the acetato-ligand and CuN_2O_2 planes, which resulted in values 52.25 ° and 67.98 ° for **8** and 60.92 ° and 66.61 ° for **9**.

Furthermore, the reliability and suitability of the DFT method used here for calculation of *J*-parameters can be judged by inspecting Fig. 12, where all the calculated *J*-values are compared to those determined by the experimental magnetic data. We can conclude that except for compound **8**, the experimental values J^{mag} are found within the intervals defined by calculated J^{Ruiz}/J^{Yam} values, which means that this procedure can reliably determine the nature of the isotropic exchange (antiferromagnetic/ferromagnetic) and also quite accurate in predicting quantitative values of *J*-parameters for this family of copper(II) dimeric complexes.

Please insert Figure 12 close to here

Experimental

Materials and physical measurements

The compound bis(2-pyridylmethyl)amine (DPA) was purchased from TCI-America. All other chemicals were commercially available and used without further purification. The ligands 2,6-bis[bis(2-pyridylmethyl)aminomethyl]-4-chlorophenol (L^{Cl}-OH) and 2,6-bis[bis(2-pyridylmethyl)aminomethyl]-4-methylphenol (L^{Me}-OH) (Chart 1) were prepared and characterized according to the published procedure.[1,2] Infrared spectra of all complexes and ligands were recorded on a JASCO FTIR-480 plus spectrometer as KBr pellets, except complex **4** was measured using

Nexus 670 spectrometer (ATR) (Thermo Nicolet, USA). Electronic spectra were recorded using an Agilent 8453 HP diode array UV-Vis spectrophotometer. ^{1}H and ^{13}C NMR spectra were obtained at room temperature on a Varian 400 NMR spectrometer operating at 400 MHz (^{1}H) and 100 MHz (^{13}C). ^{1}H and ^{13}C NMR chemical shifts (δ) are reported in ppm and were referenced internally to residual solvent resonances (DMSO-d_6: δ_H = 2.49, δ_C = 39.4 ppm). ESI-MS spectra were measured on an LC-MS Varian Saturn 2200 spectrometer. The conductivity measurements were performed using a Mettler Toledo Seven Easy conductivity meter and the cell constant was determined by the aid of 1413 μS/cm conductivity standard. The molar conductivity of the complexes were determined from $\Lambda_M = (1.0x10^3\ \kappa)/M$, where κ = cell constant and M is the molar concentration of the complex. Magnetic measurements were performed with an MPMS XL7 SQUID magnetometer (Quantum Design, Inc.) (T = 1.9–300 K at B = 1 T; B = 0–5 T at T = 2 and 5 K). The magnetic data were corrected for diamagnetic susceptibilities. Elemental analyses were carried out by the Atlantic Microlaboratory, Norcross, Georgia U.S.A.

Theoretical DFT calculations

The *ab initio* theoretical calculations were done with the ORCA 3.0 computational package[49] using the B3LYP functional[50] and polarized triple-ζ quality basis set def2-TZVP(-f) for all the complexes (including all the atoms).[51] The single-point energy calculations were done on molecular fragments based on the experimental X-ray geometries: $[Cu_2(\mu\text{-}L^{Cl}\text{-}O)(\mu\text{-}OH)(ClO_4)]^+$ of **1**, $[Cu_2(\mu\text{-}L^{Cl}O)(\mu\text{-}pz)(ClO_4)]^+$ of **2,** $[Cu_2(\mu\text{-}L^{Cl}\text{-}O)(\mu\text{-}(O_2P(OC_6H_5)_2)]^{2+}$ of **3**, $[Cu_2(\mu\text{-}L^{Cl}\text{-}O)(dca)_2]^+$ of **4**·2CH_3CN, $[Cu_2(\mu\text{-}L^{Me}\text{-}O)(dca)_2]^+$ of **5**·2CH_3CN, $[Cu_2(\mu\text{-}L^{Me}O)(\mu\text{-}OH)]^{2+}$ of **6**, $[Cu_2(\mu\text{-}L^{tBu}O)(\mu\text{-}CH_3O)]^{2+}$ of **7**, $[Cu_2(\mu\text{-}L^{Me}O)(\mu\text{-}CH_3COO)]^{2+}$ of **8** and $[Cu_2(\mu\text{-}L^{tBu}O)(\mu\text{-}CH_3COO)]^{2+}$ of **9**. All the calculations utilized the RI approximation with the decontracted auxiliary def2-TZV/J Coulomb fitting basis set and the chain-of-spheres (RIJCOSX) approximation to exact exchange.[52] Also, increased integration grids (Grid5 and GridX5 in ORCA convention) and tight SCF convergence criteria were used. The isotropic exchange parameters J were calculated by comparing the energies of high-spin (HS) and broken-symmetry (BS) spin states utilizing both Ruiz's approach[53] and Yamaguchi's approach.[54] Plots of spin densities were done by means of the VESTA 3 software.[55]

X-ray crystal structure analysis

The X-ray single-crystal data of compounds **1-5** were collected on a Bruker-AXS APEX CCD diffractometer at 100(2) K. The crystallographic data, conditions retained for the intensity data collection and some features of the structure refinements are listed in Table 2. The intensities were collected with Mo-Kα radiation (λ= 0.71073 Å). Data processing, Lorentz-polarization and absorption corrections were performed using APEX, and the SADABS computer programs.[56] The structures were solved by direct methods and refined by full-matrix least-squares methods on F^2, using the SHELXTL[57] program package. All non-hydrogen atoms were refined anisotropically. The hydrogen atoms were located from difference Fourier maps, assigned with isotropic displacement factors and included in the final refinement cycles by use of HFIX (parent C atom) or DFIX (parent O atom) utility of the SHELXTL program. Molecular plots were performed with the Mercury program.[58] In case of **2**, split occupancy of 0.508(7) and 0.492(7) were applied to disordered atoms of one pyridyl moiety.

Please insert Table 2 close to here

Caution: *Salts of perchlorate and their metal complexes are potentially explosive and should be handled with great care and in small quantities.*

Syntheses of the complexes

$[Cu_2(\mu\text{-}L^{Cl}\text{-}O)(\mu\text{-}OH)](ClO_4)_2$ ***(1).*** To a mixture of $Cu(ClO)_2{\cdot}6H_2O$ (0.152 g, 0.40 mmol) and 2,6-bis[bis(2-pyridylmethyl)aminomethyl]-4-chlorophenol (0.110 g, 0.20 mmol) dissolved in MeOH (20 mL), an aqueous solution of Na_2CO_3 (21 mg, 0.20 mmol dissolved in 3 mL H_2O) was added. The resulting green solution was heated on a steam-bath for 10 min, filtered while hot through celite and then allowed to stand at room temperature. The precipitate which was obtained was collected by filtration, washed with propan-2-ol and Et_2O and then dried at room temperature (overall yield: 105 mg, 59%). Recrystallization of the product from H_2O afforded green crystals suitable for X-ray structure determination. Characterization for **1:** Calcd for $C_{32}H_{31}Cl_3Cu_2N_6O_{10}$ (MM = 892.07 g/mol): C, 43.04; H, 3.50; N, 9.41%. Found: C, 42.96; H, 3.46; N, 9.27%. Selected IR bands (cm^{-1}): 3429 (m,b) ν(O-H); 1608 (s), 1573 (w), 1483 (m), 1466 (s), 1440 (m) (pyridyl groups); 1092 (vs, b) ν_{as}(Cl-O). UV-VIS spectrum {λ_{max}, nm (ε, $M^{-1}cm^{-1}$/Cu atom)} in CH_3CN: 805 (137, b). ESI-MS in CH_3CN: *m/z* = 835.056, 767.069, 361.037(major peaks) and for negative ion: *m/z* = 98.949 (100%). Molar conductivity, Λ_M (CH_3CN) = 267 Ω^{-1} cm^2 mol^{-1}.

$[Cu_2(\mu\text{-}L^{Cl}O)(\mu\text{-}pz)(ClO_4)]ClO_4$ ***(2).*** To a hot solution containing 2,6-bis[bis(2-pyridyl-methyl)aminomethyl]-4-chlorophenol (0.110 g, 0.20 mmol) and $Cu(ClO)_2 \cdot 6H_2O$ (0.152 g, 0.40 mmol) dissolved in MeOH (30 mL) pyrazole, Hpz (14 mg, 0.20 mmol) was added. The resulting green solution was heated on a steam-bath for 10 min, filtered while hot through celite and then allowed to stand at room temperature. The greenish-blue precipitate which was obtained after few hours was collected by filtration, washed with propan-2-ol and Et_2O and then dried at room temperature (overall yield: 160 mg, 85%). Shiny greenish-blue crystals suitable for X-ray structure determination were obtained from dilute solution. Characterization for **2:** Calcd for $C_{35}H_{33}Cl_3Cu_2N_8O_9$ (MM = 943.144 g/mol): C, 44.57; H, 3.53; N, 11.88%. Found: C, 44.38; H, 3.59; N, 11.92%. Selected IR bands (cm^{-1}): 1609 (s), 1485 (w), 1460 (m), 1447 (m), (pyridyl groups); 1120, 1093 (vs) ν_{as}(Cl-O). UV-VIS spectrum {λ_{max}, nm (ε, $M^{-1}cm^{-1}$/Cu atom)} in CH_3CN: 456 (sh), 799 (194). ESI-MS in CH_3CN: *m/z* = 821.012, 767.069, 361.035 (major peaks) and for negative ion: *m/z* = 98.950 (100%) [ClO_4^- = 99.453]. Molar conductivity, Λ_M (CH_3CN) = 298 Ω^{-1} cm^2 mol^{-1}.

$[Cu_2(\mu\text{-}L^{Cl}\text{-}O)(\mu\text{-}O_2P(OC_6H_5)_2)](ClO_4)_2$ ***(3).*** Diphenyl phosphate (50 mg, 0.20 mmol) which was neutraized with NaOH (0.2 mmol dissolved in 2 mL H_2O) was added dropwise to a warm solution containing 2,6-bis[bis(2-pyridylmethyl)aminomethyl]-4-chlorophenol (0.110 g, 0.20 mmol) and $Cu(ClO)_2 \cdot 6H_2O$ (0.152 g, 0.40 mmol) in MeOH (20 mL). The resulting green solution was heated on a steam-bath for 10 min, filtered while hot through celite and then allowed to stand at room temperature. The golden single crystals, which separated in the following day, were collected by filtration, washed with propan-2-ol and Et_2O and then dried at room temperature (overall yield: 203 mg, 90%). Characterization for **3:** Calcd for $C_{44}H_{44}Cl_3Cu_2N_6O_{13}P$ (MM = 1129.272 g/mol): C, 46.97; H, 3.58; N, 7.47%. Found: C, 47.07; H, 3.73; N, 7.58%. Selected IR bands (cm^{-1}): 1611 (m), 1488 (m), 1448 (m) (pyridyl groups); 1121, 1108, 1092 (vs) ν_{as}(Cl-O). UV-VIS spectrum {λ_{max}, nm (ε, $M^{-1}cm^{-1}$/Cu atom)} in CH_3CN: 440 (542, b). ESI-MS in CH_3CN: *m/z* = 835.060, 767.074, 361.037 (major peaks) and for negative ion: *m/z* = 98.949 (100%) [ClO_4^- = 99.453]. Molar conductivity, Λ_M (CH_3CN) = 294 Ω^{-1} cm^2 mol^{-1}.

$[Cu_2(\mu\text{-}L^{Cl}\text{-}O)(dca)_2]PF_6$ ***(4·2CH$_3$CN).*** To a hot solution containing 2,6-bis[bis(2-pyridylmethyl)aminomethyl]-4-chlorophenol (0.111 g, 0.20 mmol) and $Cu(NO_3)_2 \cdot 3H_2O$ (97 mg, 0.40 mmol) in MeOH (40 mL) sodium dicyanamide (36 mg, 0.40 mmol) dissolved in H_2O (3 mL) was added dropwise and this was followed by the addition of NH_4PF_6 (100 mg, 0.6 mmol). The resulting greenish-blue solution was heated on a steam-bath for 10 min, filtered while hot through celite and

then allowed to stand at room temperature. The crude precipitate which separated in the following day was collected by filtration and recrystallized from acetonitrile to afford shiny greenish-blue single crystals. These were filtered, washed with propan-2-ol and Et_2O and then dried at room temperature (overall yield: 122 mg, 59%). Characterization for **4**·2CH_3CN: Calcd for $C_{38}H_{36}ClCu_2F_6N_{14}OP$ (MM = 1036.341 g/mol): C, 44.04; H, 3.50; N, 18.92%. Found: C, 44.48; H, 3.53; N, 18.76%. Selected IR bands (cm^{-1}): 2283 (m), 2227 (m), 2161 (vs); 1610 (m) 1574 (w), 1483 (w), 1445 (m) (pyridyl groups); 837 (s) ν(P-F). UV-VIS spectrum {λ_{max}, nm (ε, $M^{-1}cm^{-1}$/Cu atom)} in CH_3CN: 457 (117), 656 (155, b). ESI-MS in CH_3CN: *m/z* = 835.060, 767.071, 361.039 (major peaks) and for negative ion: *m/z* = 144.965 (100%). Molar conductivity, Λ_M (CH_3CN) = 161 Ω^{-1} cm^2 mol^{-1}.

[Cu$_2$(μ-L^{Me}-O)(dca)$_2$]PF$_6$·2CH$_3$CN (5·2CH$_3$CN). This complex was prepared using a procedure similar to that described above for **4**·2CH_3CN except 2,6-bis[bis(2-pyridylmethyl)aminomethyl]-4-methylphenol was used instead of the corresponding 2,6-bis[bis(2-pyridylmethyl)aminomethyl]-4-chlorophenol. Recrystallized of the crude compound from acetonitrile afforded shiny blue well shaped single crystals (overall yield: 144 mg, 71%). Characterization for **5**·2CH_3CN: Calcd for $C_{41}H_{39}Cu_2F_6N_{14}OP$ (MM = 1015.92 g/mol): C, 48.47; H, 3.87; N, 19.30%. Found: C, 48.83; H, 4.00; N, 19.45%. Selected IR bands (cm^{-1}): 2291 (m), 2237 (m), 2173 (vs), 1637 (m), 1611 (m), 1472 (m), 1446 (m) (pyridyl groups); 844 (s) ν(P-F). UV-VIS spectrum {λ_{max}, nm (ε, $M^{-1}cm^{-1}$/Cu atom)} in CH_3CN: 479 (217), 669 (155, b). ESI-MS in CH_3CN: *m/z* = 813.113, 747.125, 351.063 (major peaks) and for negative ion: *m/z* = 144.965 (100%) [PF_6^- = 144.97]. Molar conductivity, Λ_M (CH_3CN) = 179 Ω^{-1} cm^2 mol^{-1}.

Conclusions

The reaction of copper(II) salts with 2,6-bis[bis(2-pyridylmethyl)aminomethyl]-4-substituted-phenol (L^R-OH) affords two categories of dinuclear complexes in which the phenolate ligand is bridging the two Cu(II) atoms *via* the deprotonated phenol group. The first category is the singly bridged μ-phenoxido complexes of the general formula $[Cu_2(\mu\text{-}L^R\text{-}O)(X)_2]^{+/3+}$ {R = Cl, X = dca (complex **4**); R = X = Cl^-;[1] R = CH_3, X = dca (complex **5**), R = CH_3, X = OAc^-, Cl^-, N_3^-, H_2O and CH_3CN).[2,4,5,28] This class of compounds mediates very weak antiferromagnetic coupling through the bridged phenoxido group.[1,2] The second category of the bicompartmental phenolate ligands is the doubly bridged complexes where in addition to the bridged phenoxido group, an extra bridge exists and this was observed here in this study in complexes $[Cu_2(\mu\text{-}L^R\text{-}O)(\mu\text{-}X)]^{+/2+}$ {**1**: X = OH^-, **2**: X = pz^- and **3**: X =

$O_2P(OC_6H_5)_2^-$} and in some other related complexes **6-9** {R = CH_3/*t*-Bu, X = OH-, OAc^-; R = *t*-Bu, X = OCH_3^-}.[4,28,34,47] In this case moderate ferromagnetic to very strong antiferromagnetic coupling was observed.

The DFT supported analysis of magnetic properties showed that in the case of the doubly bridged complexes **1-3** and **6-9**, the key factor determining the nature and strength of the isotropic exchange is the geometry of copper(II) chromophores (SP-SP, SP-TBP or TBP-TBP), thus mutual orientation of magnetic orbitals based on d_{x2-y2}/d_{x2-y2}, d_{x2-y2}/d_{z2} or d_{z2}/d_{z2} orbitals and efficiency of their magnetic orbital overlaps mediated by both μ-L^R-O_{ph} and μ-X bridging ligands. Therefore, the strongest antiferromagnetic exchange within the studied compounds was found in complexes **3** (X = $O_2P(OC_6H_5)_2^-$) and **7** (X = CH_3O^-), where either d_{x2-y2}/d_{x2-y2} or d_{z2}/d_{z2} orbitals resulting from SP-SP or TBP-TBP copper geometries are efficiently overlapping, whereas the strongest ferromagnetic coupling was induced in the acetato-bridged complex **9**. Moreover, the herein the DFT method used based on the B3LYP functional and def2-TZVP(-f) basis set seems to predict properly the nature and strength of the magnetic exchange almost for all the studied complexes, thus enabling us to utilize it also for other structurally similar compounds in future. The data in Table 1 revealed that magnetic exchange in the family of doubly hetero-bridged pentacoordinate copper(II) complexes cannot be simply predicted by analyzing the basic structural parameters like <(Cu-O_{Ph}-Cu) and <(Cu-X-Cu) angles but the efficiency of magnetic orbitals overlap is more critical in evaluating the variation of copper chromophores geometries (SP vs. TBP) and their mutual orientation.

†Electronic Supporting Information (ESI)

Electronic supplementary information (ESI) available: Figures S1†-S5† show the mass spectra of the complexes **1-5**, respectively whereas figures S†6–S10† are showing the corresponding packing plots for the crystal structures. Selected bond parameters of complexes **1-5** are summarized in Tables S1–S5, respectively. CCDC-1060469, 1060470, 1060471, 1060472 and 1060473 contain the crystallographic data in CIF format for **1** - **5**, respectively. These data can be obtained free of charge from The Cambridge Crystallographic Data Centre via www.ccdc.cam.ac.uk/data_request/cif. For ESI and crystallographic data in CIF file or other electronic format see DOI:10.10??????????????.

Authors information

*(S.S.M.) E-mail: ssmassoud@louisiana.edu, Tel. +01 337-482-5672, Fax: +01 337-482-5676; (Z.D.) E-mail: zdenek.travnicek@upol.cz, Tel. +420 585-634-352, Fax: +420 585-634-954; (F.A.M.) E-mail: E-mail: mautner@tugraz. at, Tel. ++43 316-4873-8234, fax: ++43 316-4873-8225.

Acknowledgements

This research was financially supported by the Department of Chemistry-University of Louisiana at Lafayette. FAM acknowledges support by NAWI Graz. ZT and RH acknowledge support by LO1305.

References

1. S. S. Massoud, M. Spell, C. Ledet, T. Junk, R. Herchel, R. C. Fischer, Z. Travnicek and F. A. Mautner, *Dalton Trans.*, 2015, **44**, 2110.
2. S. S. Massoud, T. Junk, M. Mikuriya, N. Naka and F. A. Mautner, *Inorg. Chem. Commun.*, 2014, **50**, 48.
3. (a) J. K. Bjernemose and C. J. McKenzie, *Acta Crytallogr., Sect. E., Struct. Rep. Online,* 2003, **59**, o1275; (b) G. T. Gomes, A. Hazell and C. J. McKenzie, *Acta Crytallogr., Sect. C., Crystal. Struct. Commun.*, 2000, **56**, 382.
4. Y. Nishida, H. Shimo, H. Maehara and S. Kida, *J. Chem. Soc., Dalton Trans.*, 1985, 1945.
5. F. Michel, St. P. Torelli, F. Thomas, C. Duboc, C. Philouze, C. Belle, S. Hamman, E. Saint-Aman and J.-L. Pierre, *Angew. Chem. Int. Ed.*, 2005, **44**, 438.
6. (a) K. Selmeczi, C. Michel, A. Milet, I. Gautier-Luneau, C. Philouze, J.-L. Pierre, D. Schnieders A. Rompel and C. Belle, *Chem. Eur. J.*, 2007, **13**, 9093.
7. Y. Gultneh,Y. T. Tesema, T. B. Yisgedu, R. J. Butcher, G. Wang and G. T. Yee, *Inorg. Chem.*, 2006, **45**, 3023.
8. B. Das, H. Daver, M. Pyrkosz-Bulska, E. Persch, S. K. Barman, R. Mukherjee, E. Gumienna-Kontecka, M. Jarenmark, F. Himo and E. Nordlander, *J. Inorg. Biochem.*, 2014, **132**, 6.
9. M. Jarenmark, M. Haukka, S. Demeshko, F. Tuczek, L. Zuppiroli, F. Meyer and E. Nordlander, *Inorg. Chem.*, 2011, **50**, 3866.
10. P. Comba, L. R. Gahan, V. Mereacre, G. R. Hanson, A. K. Powell, G. Schenk and M. Zajaczkowski-Fischer, *Inorg. Chem.* 2012, **51**, 12195.
11. S. Bosch, P. Comba, L. R. Gahan and G. Schenk, *Inorg. Chem.*, 2014, **53**, 9036.
12. S. Svane, F. Kryuchkov, C. J. Lennarston, C. J. McKenzie and F. Kjeldsen, *Angew Chem., Int. Ed.*, 2012, **51**, 3216.
13. S. J. Smith, C. J. Noble, R. C. Palmer, G. R. Hanson, G. Schenk, L. R. Gahan and M. J. Riley, *J. Biol. Inorg. Chem.*, 2008, **13**, 499.
14. S. Blanchard, G. Blain, E. Riviere, M. Nierlich and G. Blondin, G., *Chem. Eur. J.*, 2003, **9**, 4260.
15. L. M. Berreau, A. Saha and A. M. Arif, *Dalton Trans.*, 2006, 183.
16. S. Halder, S. Dey and C. Rizzoli, P. Roy, *Polyhedron*, 2014, **78**, 85.
17. (a) A. S. Borovik, M. P. Hendrich, T. R. Holman, E. Munck, V. Papaefthymiou and L. Junior Que, *J. Am. Chem. Soc.*, 1990, **112**, 6031; (b) A. S. Borovik and L. Junior Que, *J. Am. Chem. Soc.*, 1988, **110**, 2345.

18. T. Manago, S. Hayami, H. Oshio, S. Osaka, H. Hasuyama, R. H. Herber, K. J. Berry and Y. Maeda, *J. Chem. Soc., Dalton Trans.*, 1999, 1001.
19. H. Diril, H.-R. Chang, M. J. Nilges, X. Zhang, J. A. Potenza, H. J. Schugar, S. S. Isied and D. N. Hendrickson, *J. Am. Chem. Soc.*, 1989, **111**, 5102.
20. R. C. Holz and J. M. Brink, *Inorg.Chem.*, 1994, **33**, 4609.
21. (a) K. Matsufuji, H. Shiraishi, Y. Miyasato, T. Shiga, M. Ohba, T. Yokoyama and H. Ōkawa, *Bull. Chem. Soc. Jpn.*, 2005, **78**, 851; (b) D. Saravanakumar, N. K. Sengottuvelan, G. Priyadarshni, M. Kandaswamy and H. Ōkawa, *Polyhedron,* 2004, **23**, 665.
22. L. F. Taylor and O. P. Anderson, *J. Am. Chem. Soc.*, 1988, **110**, 1986.
23. M. Suzuki, M. Mikuriya, S. Murata, A. Uehara and H. Oshio, *Bull. Chem. Soc. Jpn.*, 1987, **60**, 4305.
24. J. J. Maloney, M. Glogowski, D. F. Rohrbach and F. L. Urbach, *Inorg. Chim. Acta*, 1987, **127**, L33.
25. (a) R. K. Edgal, A. D. Bond and C. J. Mckenzie, *Dalton Trans.*, 2009, 3833; (b) R. K. Edgal, F. B. Larsen, A. D. Bond, C. J. Mckenzie, C. J. *Inorg. Chim. Acta*, 2005, **358**, 376.
26. T. N. Sorrell, D. L. Jameson and C. J. O'Connor, *Inorg. Chem.,* 1984, **23**, 190.
27. A. Biswas, L. K. Das and A. Ghosh, *Polyhedron,* 2013, **61**, 253.
28. S. Torelli, C. Belle, I. Gautier-Luneau, J. L. Pierre, E. Saint-Aman, J. M. Latour, L. Le Pape and D. Luneau, *Inorg. Chem.*, 2000, **39***,* 3526.
29. N. A. Rey, A. Neves, A. J. Bortoluzzi, C. T. Pich and H. Terenzi, *Inorg. Chem.*, 2007, **46**, 348.
30. L. J. Daumann, J. A. Larrabee, P. Comba, G. Schenk and L. R. Gahan, *Eur. J. Inorg. Chem.,* 2013, 3082.
31. (a) T. P. Camargo, F. F. Maia, C. Chaves, B. de Souza, A. J. Bortoluzzi, N. Castilho, T. Bortolotto, H. Terenzi, E. E. Castellano, W. Haase, Z. Tomkowicz, R. A. Peralta and A. Neves, *J. Inorg. Biochem.*, 2015, **146**, 77.
32. A. Neves, M. Lanzanaster, A. J. Bortoluzzi, R. A. Peralla, A. Cassellato, E. E. Castellano, P. Herrald, M. J. Riley and G. Schenk, *J. Chem. Soc.* 2007, **129**, 7486.
33. M. Ghiladi, C. J. Mckenzie, A. Meler, A. K. Powell, J. Ulstrup and S. Wocadlo, *J. Chem. Soc., Dalton Trans.*, 1997, 4011.
34. P. Dalgaard, A. Hazell, C. J. McKenzie, B. Moubaraki and K. S. Murray, *Polyhedron*, 2000, **19**, 1909.
35. S. Sarkar, S. Majumder, S. Sasmal, L. Carrella, E. Rentschler and S. Mohanta, *Polyhedron*, 2013, **50**, 270.
36. C. Belle, C. Beguin, I. Gautler-Luneau, S. Hamman, C. Phllouze, J. L. Pierre, F. Thomas, S. Torrelli, S. Saint-Aman and M. Bonin, *Inorg. Chem.* 2002, **41**, 479.
37. F. B. Johansson, A. D. Bond, U. G. Nilsen, B. Maubaraki, K. S. Murray, K. J. Berry, J. A. Larrabee and C. J. McKenzie, *Inorg. Chem.*, 2008, **47**, 5079.
38. H. Kohler, A. Kolbe and G. Z. Lux, *Anorg. Allg. Chem.*, 1977, **428**, 103.
39. (a) S. S. Massoud, A. E. Guilbeau, H. T. Luong, R. Vicente, J. H. Albering, R. C. Fischer and F. A. Mautner, *Polyhedron*, **2013**, 54, 26; (b) S. S. Massoud, M. C. Lemieux, L. L. Le Quan, R. Vicente, J. H. Albering, F. A. Mautner, *Inorg. Chim. Acta*, 2012, **388**, 71; (c) F. A. Mautner, J. H. Albering, R. Vicente, F. R. Louka, A. A. Gallo and S. S. Massoud, *Inorg. Chim. Acta*, 2011, **365**, 290; (d) F. A. Mautner, J. B. Soileau, P. K. Bankole, A. A. Gallo and S. S. Massoud, *J. Mol. Struct.,* 2008, **889**, 271.
40. (a) S. S. Massoud, R. S. Perkins, F. R. Louka, W. Xu, A. Le Roux, Q. Dutercq, Q.; R. C. Fischer, F. A. Mautner, M. Handa, Y. Hiraoka, G. L. Kreft, T. Bortolotto and H. Terenzi, *Dalton Trans.*,

2014, **43**, 10086; (b) F. R. Louka, A. D. Stewart, E. Regel, F. A. Mautner, S. Demeshko, F. Meyer and S. S. Massoud, *Inorg. Chem. Commun.*, 2012, **22**, 60; (c) S. S. Massoud, F. A. Mautner, F. R. Louka, S. Demeshko, S. Dechert, F. Meyer, *Inorg. Chim. Acta*, 2011, **370**, 435.

41. B. J. Hathaway in *Comprehensive Coordination Chemistry*, ed. G. Wilkinson, R. D. Gillard and J. A. McCleverty, Pergamon Press, Oxford, England, 1987, vol. 5, p. 533.
42. (a) S. S. Massoud, F. R. Louka, R. N. David, M. J. Dartez, Q. L. Nguyn, N. J. Labry, R. C. Fischer and F. R. Mautner, *Polyhedron*, 2015, **90**, 258; (b) F. A. Mautner, M. Mikuriya, Y. Naka, F. R. Louka and S. S. Massoud, *Polyhedron* 2015, **85**, 110; (c) S. S. Massoud, L. Le Quan, K. Gatterer, J. H. Albering, R. C. Fischer and F. A. Mautner, *Polyhedron*, 2012, **31**, 601; (d) F. A. Mautner, J. H. Albering, E. V. Harrelson, A. A. Gallo and S. S. Massoud, *J. Mol. Struct.,* 2011, **1006**, 570; (e) M. Schatz, M. Becker, F. Thaler, F. Hampel, S. Schindler, R. R. Jacobson, Z. Tyeklár, N. N. Murthy, P. Ghosh, Q. Chen, J. Zubieta and K. D. Karlin, *Inorg. Chem.*, 2001, **49**, 2312.
43. T. N. Sorrell, *Tetrahedron*, 1999, **45**, 3.
44. l. J. Daumann, P. Comba, J. A. Larrabee, G. Schenk, R. Stranger, G. Cavigliasso and L. R. Gahan, *Inorg. Chem.*, 2013, **52**, 2029.
45. A. W. Addison, T. N. Rao, J. Reedijk, J. V. Rijin and G. C. Verschoor, *J. Chem. Soc., Dalton Trans.*, 1984, 1349.
46. R. Boča, A Handbook of Magnetochemical Formulae, Elsevier, Amsterdam, 2012.
47. S. S. Massoud, T. Junk, R. Herchel, Z. Trávníček, M. Mikuriya, R. C. Fischer and F. A. Mautner, *Inorg. Chem. Commun.*, 2015, **60**, 1.
48. J. Pasan, F. S. Delgado, Y. Rodriguez-Martin, M. Hernandez-Molina, C. Ruiz-Perez, J. Sanchiz, F. Lloret and M. Julve, *Polyhedron*, 2003, **22**, 2143.
49. F. Neese, *WIREs Comput. Mol. Sci.*, 2012, **2**, 73.
50. (a) C. Lee, W. Yang and R. G. Parr, *Phys. Rev. B*, 1988, **37**, 785; (b) A. D. Becke, *J. Chem. Phys*., 1993, **98**, 1372; (c) A. D. Becke, *J. Chem. Phys.*, 1993,**98**, 5648; (d) P. J. Stephens, F. J. Devlin, C. F. Chabalowski and M. J. Frisch, *J. Phys. Chem.*, 1994, **98**, 11623.
51. (a) A. Schaefer, H. Horn and R. Ahlrichs, *J. Chem. Phys.*, 1992, **97**, 2571; (b) A. Schafer, C. Huber and R. J. Ahlrichs, *Chem. Phys.*, 1994, **100**, 5829; (b) F. Weigend and R. Ahlrichs, *Phys. Chem. Chem. Phys.*, 2005, **7**, 3297.
52. F. Neese, F. Wennmohs, A. Hansen and U. Becker, *Chem. Phys.*, 2009, **356**, 98.
53. (a) E. Ruiz, J. Cano, S. Alvarez and P. Alemany, *J. Comput. Chem.*, 1999, **20**, 1391; (b) E. Ruiz, A. Rodríguez-Fortea, J. Cano, S. Alvarez and P. Alemany, *J. Comput. Chem.*, 2003, **24**, 982.
54. (a) K. Yamaguchi, Y. Takahara and T. Fueno, in V. H. Smith (Ed.), *Applied Quantum Chemistry*, Reidel, Dordrecht, 1986, p. 155; (b) T. Soda, Y. Kitagawa, T. Onishi, Y. Takano, Y. Shigeta, H. Nagao, Y. Yoshioka and K. Yamaguchi, *Chem. Phys. Lett.*, 2000, **319**, 223.
55. K. Momma and F. Izumi, VESTA 3 for three-dimensional visualization of crystal, volumetric and morphology data, *J. Appl. Crystallogr.*, 2011, 44, 1272.
56. (a) Bruker (2005) SAINT v. 7.23; Bruker AXS Inc., Madison, Wisconsin, USA; (b) G. M. Sheldrick (2001), SADABS v. 2. University of Goettingen, Germany.
57. G. M. Sheldrick, *Acta Crystallogr.,* 2008, **A64**, 112.
58. C. F. Macrae, P. R. Edington, P. McCabe, E. Pidcock, G. P. Shields, R. Taylor, T. Towler and J. van de Streek, *J. Appl. Cryst.*, 2006, **39**, 453.

TABLES

Table 1 The DFT-calculated net Mulliken spin densities (ρ), expected values $\langle S^2 \rangle$, overlap $S_{\alpha\beta}$ between the corresponding orbitals and isotropic exchange parameters (J) from high-spin (HS) and broken symmetry spin (BS) states of the dinuclear molecular fragments based on X-ray structures of **1-9** completed with selected structural parameters.

	1	**2**	**3**	**4**	**5**	**6**	**7**	**8**	**9**
ρ^{HS}(Cu1)/ρ^{HS}(Cu2)	0.63/0.64	0.61/0.62	0.64/0.63	0.61/0.61	0.61/0.61	0.63/0.63	0.63/0.63	0.61/0.61	0.61/0.61
ρ^{BS}(Cu1)/ρ^{BS}(Cu2)	-063/0.63	-0.60/0.62	-0.63/0.62	-0.61/0.61	-0.61/0.61	-0.63/0.62	-0.62/0.62	-0.61/0.61	-0.60/0.61
$\langle S^2_{HS} \rangle$	2.00	2.01	2.01	2.01	2.01	2.01	2.00	2.01	2.01
$\langle S^2_{BS} \rangle$	1.00	1.00	0.99	1.01	1.01	0.99	0.97	1.00	1.01
$S_{\alpha\beta}$	0.09278	0.07118	0.13903	0.00258	0.00272	0.13427	0.18057	0.02449	0.00894
Δ/cm^{-1}	-43.150	-46.816	-194.931	-0.031	-0.067	-142.538	-310.304	15.762	26.894
J^{Ruiz}/cm^{-1}	-43.1	-46.8	-194.9	-0.03	-0.06	-142.5	-310.3	15.8	26.9
J^{Yam}/cm^{-1}	-85.5	-93.2	-382.3	-0.06	-0.14	-279.9	-600.8	31.5	53.8
J^{mag}/cm^{-1}	-58.2/-237[a]	-61.5	-279	-0.26	-0.09	-224[b]	-312[b]	-80	30.8
type of X-bridge[c]	μ-OH	μ_2-$C_3H_3N_2$	μ_2-($PO_2(OC_6H_5)_2$)	none	none	μ-OH	μ-CH_3O	μ-CH_3COO	μ-CH_3COO
τ(Cu1)/ τ(Cu2) [d]	0.15/0.14	0.78/0.21	0.09/0.16	0.05/0.07	0.05/0.04	0.60/0.36	0.73/0.72	0.22/0.22	0.12/0.21
magnetic orbitals	d_{x2-y2}/d_{x2-y2}	d_{z2}/d_{x2-y2}	d_{x2-y2}/d_{x2-y2}	d_{x2-y2}/d_{x2-y2}	d_{x2-y2}/d_{x2-y2}	d_{z2}/d_{x2-y2}	d_{z2}/d_{z2}	d_{x2-y2}/d_{x2-y2}	d_{x2-y2}/d_{x2-y2}
<(Cu-X-Cu)/° [e]	103.29	112.01	118.04	-	-	102.10	102.40	61.08	63.43
<(Cu-O_{Ph}-Cu)/°	93.7	108.88	126.91	136.82	137.65	95.66	93.45	119.50	121.28
<(Cu-D1-D2-Cu)/° [f]		31.73	60.78					56.28	59.91
d(Cu-Cu)/10^{-10} m	3.030	3.464	3.588	4.073	4.049	2.966	3.002	3.548	3.603

[a] J-values are estimated from maxima of molar susceptibility. [b] J-values were reported in ref. 28, 34 and scaled according to eq.1. [c] see Chart 1. [d] the τ-parameters were calculated by assuming pentacoordination of copper atoms, hence neglecting semi-coordination of the perchlorate anion in **1** and **2**. [e] in the case of **2-3** and **8-9**, the angle was calculated between two bonds Cu–D1 and Cu–D2, where D1 and D2 are donor atoms of bridging ligand X. [f] in the case of **2-3** and **8-9,** the dihedral angle was calculated between Cu–D1-D2–Cu atoms, where D1 and D2 are donor atoms of the bridging ligand X.

Table 2 Crystallographic data and processing parameters for **1** – **5** compounds

Compound	**1**	**2**	**3**
Empirical formula	$C_{32}H_{30}Cl_3Cu_2N_6O_{10}$	$C_{35}H_{33}Cl_3Cu_2N_8O_9$	$C_{44}H_{40}Cl_3Cu_2N_6O_{13}P$
Formula mass	892.07	943.14	1125.24
System	Monoclinic	Monoclinic	Monoclinic
Space group	$P2_1/c$	$P2_1/c$	$P2_1/c$
a (Å)	14.958(3)	16.3363(10)	9.9409(11)
b (Å)	10.770(2)	10.3267(6)	42.116(5)
c (Å)	23.043(7)	23.9249(15)	10.8358(10)
α (°)	90	90	90
β (°)	103.386(11)	106.810(2)	103.104(5)
γ (°)	90	90	90
V (Å^3)	3611.3(15)	3863.7(4)	4418.5(8)
Z	4	4	4
T (K)	100(2)	100(2)	100(2)
μ (mm^{-1})	1.465	1.373	1.256
D_{calc} (Mg/m^3)	1.641	1.621	1.691
Crystal size (mm)	0.22 x 0.19 x 0.13	0.28 x 0.23 x 0.17	0.28 x 0.23 x 0.17
θ max (°)	25.50	26.80	25.30
Data collected	6771	40785	69771
Unique refl. / R_{int}	6771 / ----	8253 / 0.0435	7989 / 0.0994
Parameters / Restraints	505 / 6	578 / 0	622 / 0
Goodness-of-Fit on F^2	1.172	1.204	1.348
R1 / wR2 (all data)	0.0661 / 0.1957	0.0986 / 0.2343	0.0764 / 0.2165
Residual extrema (e/Å^3)	1.67 / -0.93	1.23 / -1.27	1.46 / -0.78

Table 1. cont.

Compound	**4**·2MeCN	**5**·2MeCN
Empirical formula	$C_{40}H_{36}ClCu_2F_6N_{14}OP$	$C_{41}H_{39}Cu_2F_6N_{14}OP$
Formula mass	1036.35	1015.93
System	Orthorhombic	Orthorhombic
Space group	*Pna2₁*	*Pna2₁*
a (Å)	16.2623(7)	16.2326(5)
b (Å)	12.0018(5)	12.0277(4)
c (Å)	21.7768(9)	21.8320(7)
α (°)	90	90
β (°)	90	90
γ (°)	90	90
V ($Å^3$)	4250.3(3)	4262.5(2)
Z	4	4
T (K)	100(2)	100(2)
μ (mm^{-1})	1.181	1.115
D_{calc} (Mg/m^3)	1.620	1.583
Crystal size (mm)	0.27 x 0.23 x 0.12	0.24 x 0.19 x 0.17
θ max (°)	26.500	29.030
Data collected	70106	55430
Unique refl. / R_{int}	8660 / 0.0863	11115 / 0.0652
Parameters / Restraints	589 / 1	589 / 1
Goodness-of-Fit on F^2	1.115	0.920
R1 / wR2 (all data)	0.0653 / 0.1893	0.0373 / 0.0775
Residual extrema ($e/Å^3$)	0.81 / -1.13	0.50 / -0.48

Figures and their Legends

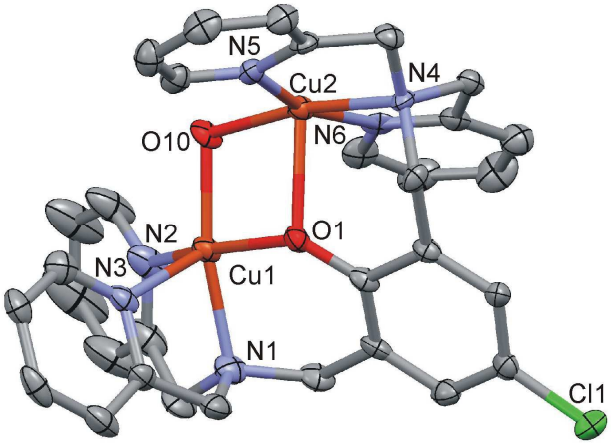

Fig. 1 Perspective view and atom numbering scheme of the complex cation, $[Cu_2(L^{Cl}O)(\mu\text{-}OH)]^{2+}$ of complex **1**. H-atoms are omitted for clarity.

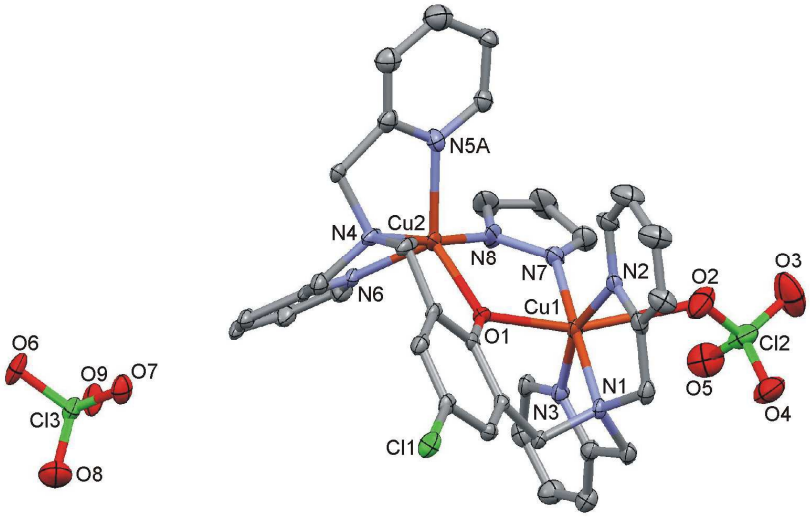

Fig. 2 Perspective view and atom numbering scheme of the complex $[Cu_2(L^{Cl}O)(\mu\text{-}pz)(ClO_4)]ClO_4$ **(2).** H-atoms are omitted for clarity.

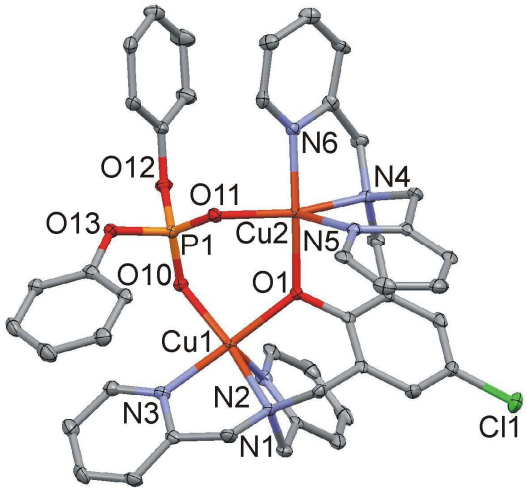

Fig. 3 Perspective view and atom numbering scheme of the dinuclear unit, $[Cu_2(L^{Cl}\text{-}O)(\mu\text{-}(PO_2(OC_6H_5)_2)]^{2+}$ of complex **3**. H-atoms are omitted for clarity.

a) **b)**

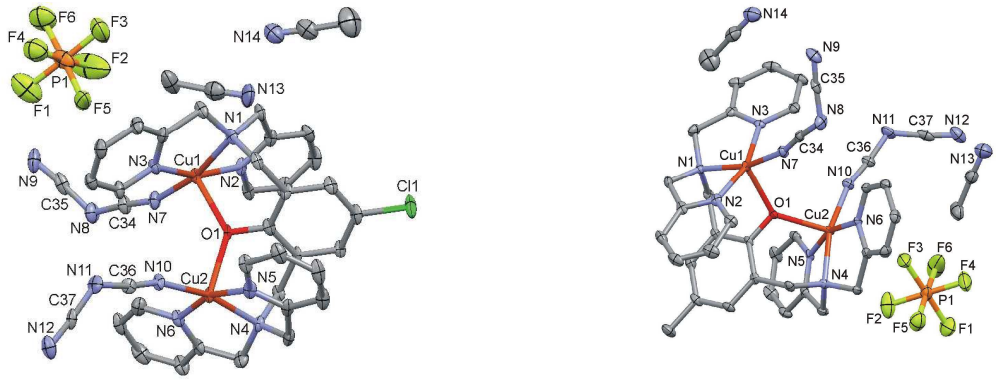

Fig. 4 Perspective views and atom numbering schemes of the dicyanamido complexes: **(a)** $[Cu_2(L^{Cl}O)(dca)_2]PF_6\cdot 2CH_3CN$ **(4**·2CH_3CN**)** and **(b)** $[Cu_2(L^{Me}O)(dca)_2]PF_6\cdot 2CH_3CN$ **(5**·2CH_3CN**).** H-atoms are omitted for clarity.

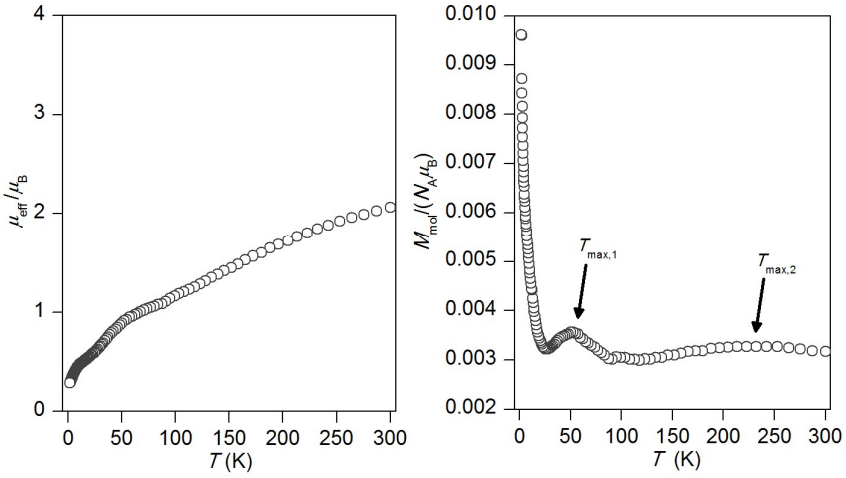

Fig. 5 The magnetic data for complex **1**: the temperature dependence of the effective magnetic moment (left) and molar magnetization measured at B = 1 T (right). The arrows point to maxima found at $T_{max,1}$ = 52.3 K and $T_{max,2}$ = 213 K.

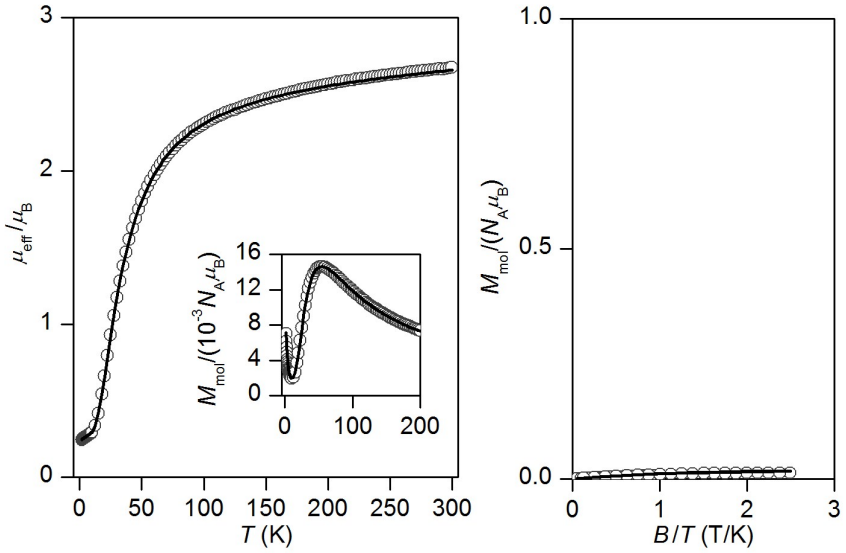

Fig. 6 The magnetic data for **2**. *Left*: the temperature dependence of the effective magnetic moment and molar magnetization measured at B = 1 T. *Right*: the isothermal magnetizations measured at T = 2 and 5 K. Open circles – experimental data, solid lines – calculated data using the equation 1 with J = -61.5 cm^{-1}, g = 2.14, χ_{TIP} = 3.9·10^{-9} m^{3}mol^{-1}, χ_{PI} = 0.85%.

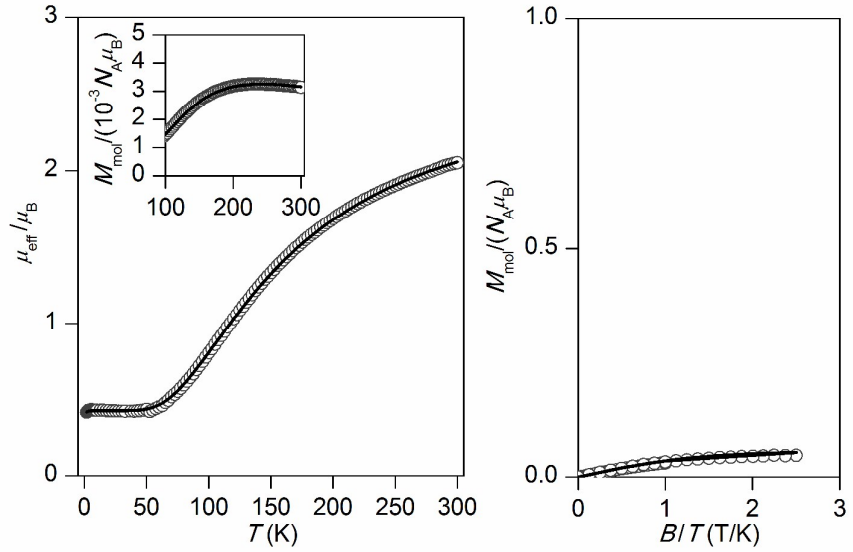

Fig. 7 The magnetic data for **3**. *Left*: the temperature dependence of the effective magnetic moment and molar magnetization measured at B = 1 T. *Right*: the isothermal magnetizations measured at T = 2 and 5 K. Open circles – experimental data, solid lines – calculated data using the equation 1, with J = -279 cm^{-1}, g = 2.17, χ_{TIP} = 0.0·10^{-9} m^{3}mol^{-1}, χ_{PI} = 2.60%.

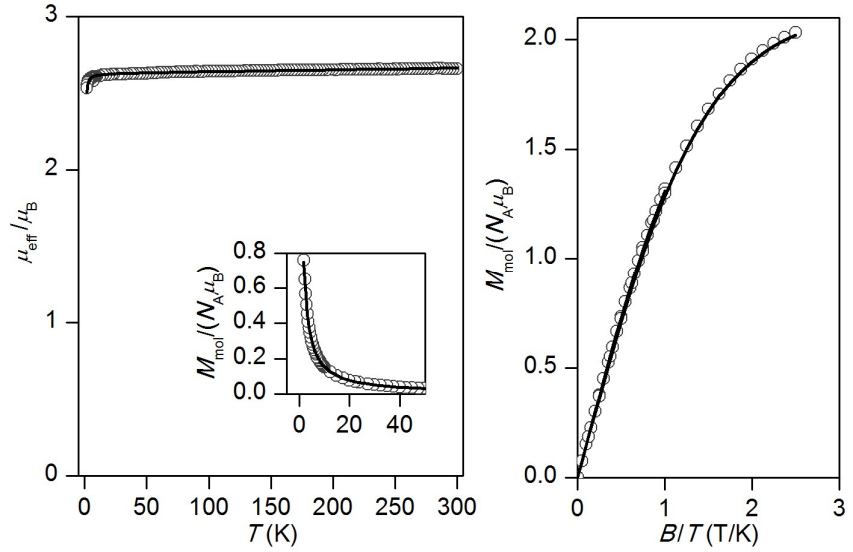

Fig. 8 The magnetic data for **4**. *Left*: the temperature dependence of the effective magnetic moment and molar magnetization measured at B = 1 T. *Right*: the isothermal magnetizations measured at T = 2 and 5 K. Open circles – experimental data, solid lines – calculated data using the equation 1, with J = -0.26 cm^{-1}, g = 2.15, χ_{TIP} = 1.0·10^{-9} m^{3}mol^{-1}.

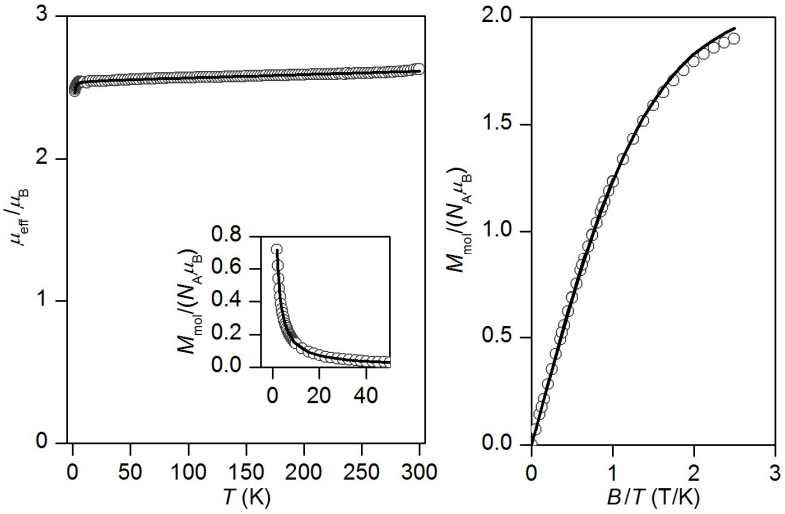

Fig. 9 The magnetic data for **5**. *Left*: the temperature dependence of the effective magnetic moment and molar magnetization measured at B = 1 T. *Right*: the isothermal magnetizations measured at T = 2 and 5 K. Open circles – experimental data, solid lines – calculated data using the equation 1, with J = -0.11 cm^{-1}, g = 2.08, χ_{TIP} = $1.9 \cdot 10^{-9}$ m^3mol^{-1}.

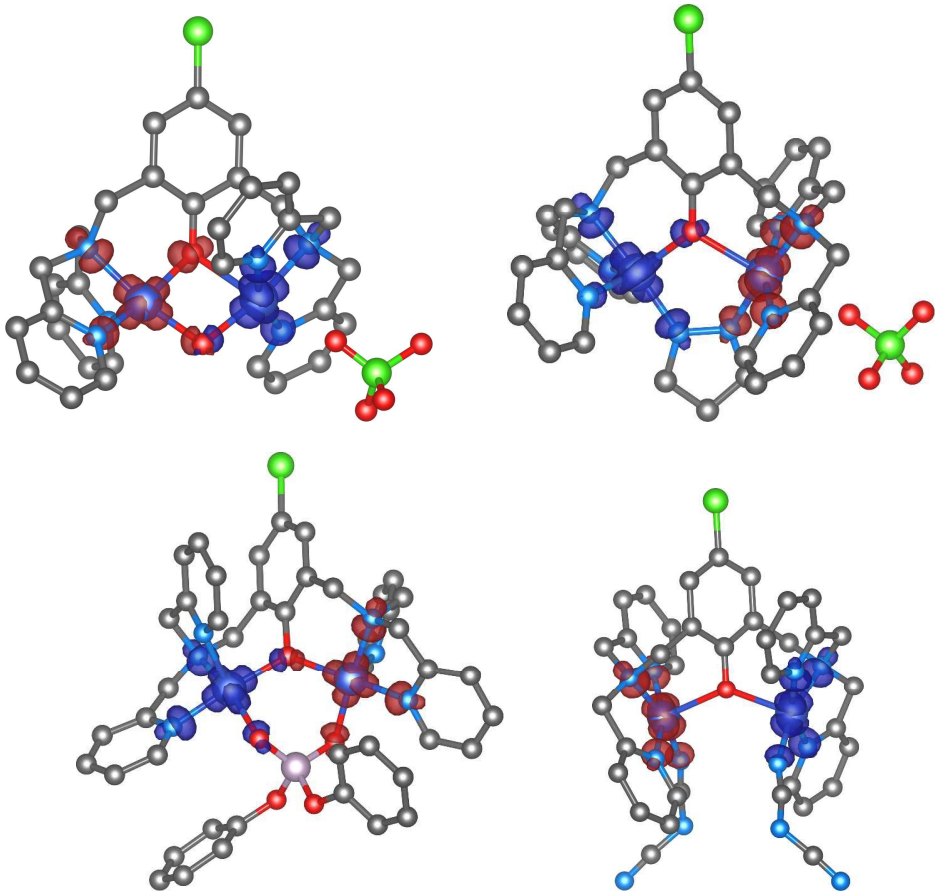

Fig. 10 The calculated the isodensity surfaces of the broken symmetry spin states using B3LYP/def2-TZVP(-f) for molecular fragments of **1-4**. Positive and negative spin densities are represented by dark blue, and dark red surfaces, respectively. Hydrogen atoms were omitted for clarity.

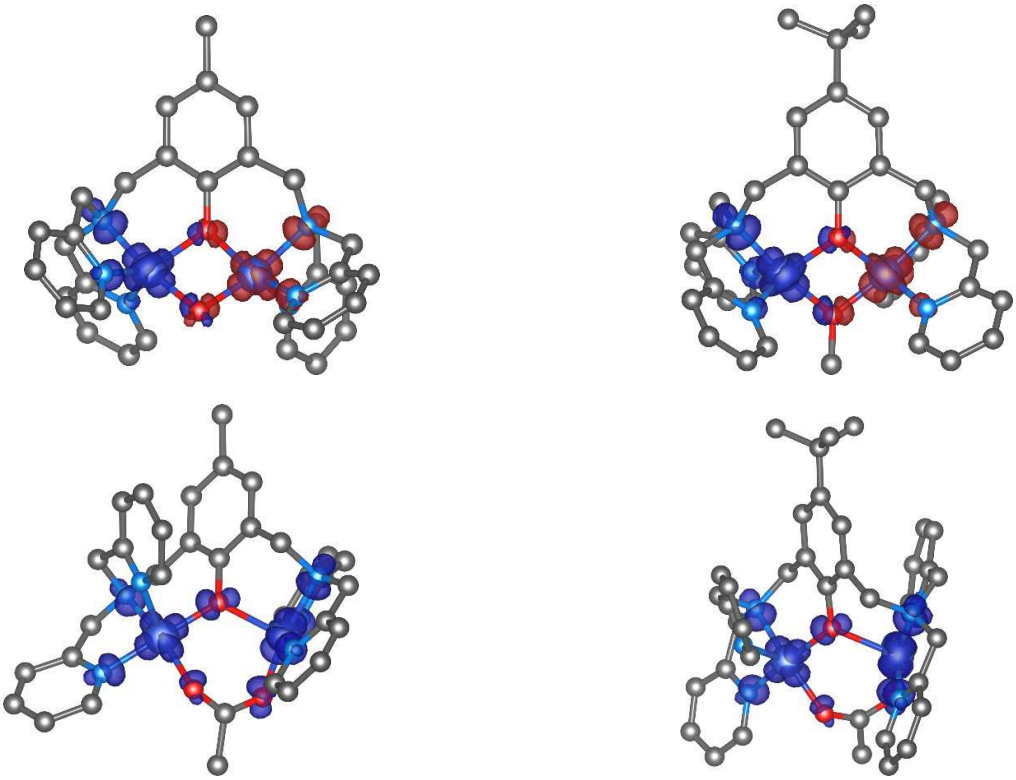

Fig. 11 The calculated isodensity surfaces of the broken symmetry spin states for molecular fragments of **6** and **7** and high spin states for molecular fragments of **8** and **9** using B3LYP/def2-TZVP(-f). Positive and negative spin densities are represented by dark blue, and dark red surfaces, respectively. Hydrogen atoms were omitted for clarity.

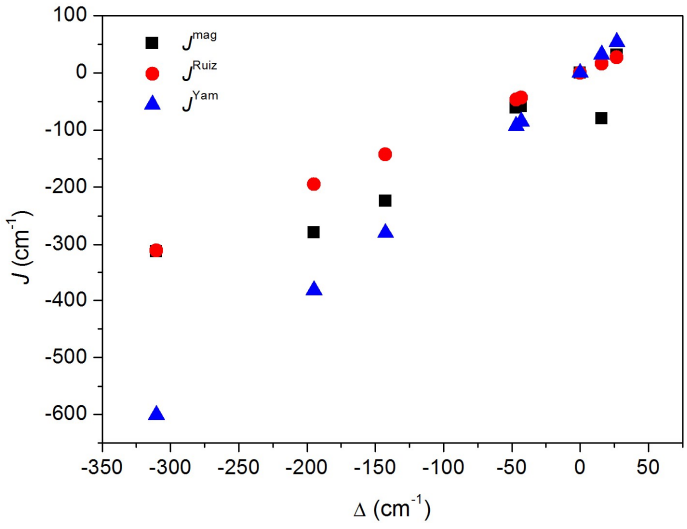

Fig. 12 Comparison of the experimentally (J^{mag}) and theoretically (J^{Ruiz} and J^{Yam}) determined isotropic exchange parameters *vs*. calculated energy difference Δ, ($\Delta = E_{BS} - E_{HS}$).